Influence of the carbon chain length of a sulfate-based surfactant on the formation of CO 2 , CH 4 and CO 2 –CH 4 gas hydrates

Christophe Dicharry, Joseph Diaz, Jean-Philippe Torre, M. Ricaurte

Influence of the carbon chain length of a sulfate-based surfactant on the formation of CO_2, CH_4 and CO_2–CH_4 gas hydrates

Christophe Dicharry [*], Joseph Diaz, Jean-Philippe Torré, Marvin Ricaurte [1]

Univ. Pau & Pays Adour, CNRS, TOTAL – UMR 5150 – LFC-R – Laboratoire des Fluides Complexes et leurs Réservoirs, Avenue de l'Université, BP 1155, Pau F-64013, France

- Surfactants may strongly promote hydrate formation under quiescent conditions.
- The promotion effect depends on the surfactant chain length.
- The promotion effect drastically reduces in the presence of CO_2.
- The presence of CO_2 influences the hydrate growth pattern.

ABSTRACT

This study investigates how the length of the carbon chain of homologous surfactants affects the amount and growth rate of gas hydrates formed in quiescent CO_2/CH_4/water systems. The hydrate formation experiments were conducted using sodium alkyl sulfates with different carbon chain lengths (C_8, C_{10}, C_{11}, C_{12}, C_{13}, C_{14}, C_{16} and C_{18}), at a concentration of 10.4 mol m^{-3}. The CO_2:CH_4 ratios investigated were 0:100, 25:75, 75:25, and 100:0. Hydrate formation was studied in a batch reactor at an initial subcooling of about 5 K. It was observed to be efficient only for those surfactants that promote the formation of a water wettable porous hydrate structure, which spreads over the inner sidewalls of the hydrate formation cell. For the CO_2:CH_4 ratios of 0:100, 25:75, 75:25 and 100:0, hydrate formation was efficient for the surfactants with respectively 8 to 14, 11 to 13, 11 to 12, and 12 carbon atoms in their alkyl chain. Only the surfactant with 12 carbon atoms was found to promote and accelerate hydrate growth for all the gas phase compositions tested. The much lesser surfactant effect on hydrate growth rate observed with the increase in the initial CO_2 fraction in the gas phase is ascribed to a modification of the adsorption behavior of the surfactant molecules on the hydrate surface, which, as already suggested by Zhang et al. (2010), is probably due to competitive adsorption between the surfactant anions and bicarbonate.

1. Introduction

Gas hydrates are nonstoichiometric crystalline compounds, composed of hydrogen bonded water molecules forming cavities within which small molecules are trapped (Sloan and Koh, 2008). They usually form at low temperatures (typically a few degrees above 273 K) and high pressure (typically a few MPa). Their high latent heat of fusion combined with their capacity both to encapsulate large amounts of gas and to selectively remove certain components from gas mixtures render gas hydrates potentially useful in various industrial processes. Applications include refrigeration (Clain et al., 2012), energy storage (Belosludov et al., 2007), energy transportation (Gudmundsson et al., 1999), capture of greenhouse gases (Adeyemo et al., 2010), and gas separation (Ricaurte et al., 2014a). Achieving formation of a large amount of hydrate at a high enough rate is generally one of the key challenges for ensuring the economic viability of gas hydrate based processes. The usually slow nucleation and growth of a gas hydrate can be accelerated, for instance, by mechanically mixing the fluids, bubbling the gas phase into the water phase or confining the water phase in a porous medium (Kang and Lee, 2010; Linga et al., 2010). All these techniques are aimed at maximizing the area of contact between the gas and water phases, and thereby the places where hydrate can form and grow. The promotion effect may also be achieved by using chemical additives, mostly surfactants. Efficient

surfactants may avoid using any agitation for hydrate formation (i.e., hydrate formation can be conducted under quiescent conditions), and thus allow to save energy costs, which is an important point if the hydrate process is to be scaled up and used industrially (Linga et al. 2010). The anionic surfactant SDS (sodium dodecyl sulfate, referred to as $SC_{12}S$ in the rest of the study) has been widely studied in the literature for its propensity to promote hydrate nucleation and growth (Kumar et al., 2015). The enhanced hydrate nucleation could be due to a favorable arrangement of the water molecules around the $SC_{12}S$ molecules (Lo et al., 2010; Lo et al., 2012). It has been demonstrated that $SC_{12}S$ micelles are not needed to boost hydrate nucleation (Watanabe et al., 2005a; Zhang et al., 2007a; Alberti et al., 2012). In fact, the temperatures used to form hydrates are in most cases away below the Krafft temperature of $SC_{12}S$. At these temperatures, $SC_{12}S$ molecules cannot form micelles, even if the $SC_{12}S$ concentration in the system is greater than the critical micelle concentration (CMC) under ambient conditions.

The enhanced hydrate growth obtained in the presence of a surfactant is very often correlated with the formation of a porous hydrate layer that grows at the water/gas (w/g) interface and spreads over the reactor wall above it (Gayet et al., 2005; Watanabe et al., 2005a; Okutani et al., 2008; Yoslim et al.,2010; Wang et al., 2015). The capillary suction of the "free water" (i.e. the water from the bulk water phase) induced by the growing hydrate porous structure results in continuous renewal of the w/g interface at the crystallization front that fosters further hydrate growth. This hydrate formation mechanism is often referred to as "capillarity driven" (Okutani et al., 2008).

Surfactants can have a remarkable effect on the hydrate formation behavior especially in the absence of mechanical agitation (i.e. under quiescent conditions) (Gayet et al., 2005; Watanabe et al., 2005a; Okutani et al., 2008; Yoslim et al., 2010; Wang et al., 2015). However, their effectiveness can be drastically impacted (positively or negatively) by different parameters such as the salinity of the aqueous phase, the nature of the gas phase, the type of the surfactant head group and the surfactant alkyl chain length (Daimaru et al., 2007; Yoslim et al.,2010; Daniel David et al., 2015; Wang et al., 2015; Jia et al.,2016).

In a recent work (Ricaurte et al., 2014b), we found that $SC_{12}S$ was the only surfactant among the sodium alkyl sulfates tested (SC_8S, $SC_{10}S$, $SC_{12}S$, $SC_{14}S$, $SC_{16}S$ and $SC_{18}S$) that promotes hydrate growth in a *quiescent* $CO_2(75$ mol%) $CH_4(25$ mol%)/water system. The aim of the present work was to study the promotion capacity of the same surfactants (with in addition two new surfactants ($SC_{11}S$ and $SC_{13}S$)) at a fixed concentration with varying gas phase compositions (pure CO_2, pure CH_4, and a mixture of 25 mol% CO_2 and 75 mol% CH_4). The chosen composition of the gas mixture used in this work is of particular interest to the studies focused on CO_2 removal from biogas and reservoir gas, as the proportion of CO_2 in biogas is generally lower than 50 vol% (Rasi et al., 2007), but can reach values higher than 70 vol% in a gas reservoir (Hanif et al. 2002). All the experiments were conducted under *quiescent conditions* and at the same initial subcooling, ΔT_{sub} (difference between the equilibrium temperature and the experiment temperature at the pressure at which the hydrate crystallization starts), of 5.0 ± 0.3 K. It will be shown that: i) depending on the composition of the gas phase, the surfactant's capacity to promote hydrate growth may be strongly affected by adding/removing a CH_2 group to/from its alkyl chain, and ii) the surfactant effect drastically decreases as the initial CO_2 fraction in the gas phase is increased.

2. Materials and methods

2.1. Materials

The gases used to form the hydrates were CO_2 (purity 99.995 mol%), CH_4 (purity 99.9995 mol%), and two gas mixtures of CO_2 and CH_4 (one referred to as 75:25, which contained 75.02 ± 0.50 mol% CO_2 and 24.98 ± 0.50 mol% CH_4, and the other referred to as 25:75, which contained 24.99 ± 0.5 mol% CO_2 and 75.01 ± 0.5 mol% CH_4). All the gases were supplied by Air Liquide. Pure water (resistivity of 18.2 MΩ cm) produced by a laboratory water purification system from Purelab was used to prepare the surfactant solutions. Tetrahydrofuran (THF) (purity $> 99.9\%$), which was used in our experiments to trigger hydrate crystallization (Ricaurte et al., 2014c), was supplied by Sigma Aldrich, and $SC_{12}S$ (purity $> 98\%$) by Chem Lab. The other SC_xS (purity 99%, except for $SC_{14}S$ which has purity of 95%) were supplied by Alfa Aeser. Table 1 gives the values of the critical micelle concentration (CMC) in pure water at 298 K, the Krafft temperature (T_k) determined in this study for each surfactant (see below the paragraph on "Krafft point determination") and the surfactant concentration [C] in the system along with the surfactant monomer concentration $[C]_{effective}$ at the temperature of 275 K (noted below T_{targ}) used for hydrate formation. Because [C] is lower than the CMC of the surfactants having a carbon chain length with less than 12 carbon atoms, $[C]_{effective}$ is equal to the *total* surfactant concentration [C] ($= 10.4$ mol m^{-3}) for these surfactants. On the other hand, for the surfactants with more than 11 carbon atoms in their alkyl chain, $[C]_{effective}$ is lower than [C] and equal to the solubility beyond which the surfactant molecules form a hydrated solid in the aqueous phase (Watanabe et al., 2005b). This occurs because both [C] is greater than the CMC of these surfactants, and T_{targ} lower than their Krafft point (T_k).

2.2. Krafft point determination

The Krafft point (i.e. the temperature below which the surfactants cannot form micelles) was determined for each surfactant using a step heating method. Test tubes containing 10.0 ± 0.1 cm^3 of the surfactant solutions at a concentration of $10 \times$ CMC (at ambient temperature) were placed in a temperature controlled bath at 274 K ($< T_{targ}$). Under these conditions of temperature and concentration, all surfactants except for SC_8S formed precipitates. The bath temperature was maintained at 274 K for 24 h then increased by a step of 1 K every 24 h until all the surfactant solutions

Table 1
Critical micelle concentrations (from literature data (Rosen and Kunjappu, 2012)) and Krafft temperatures (measured in this work) of the sodium alkyl sulfates, and the surfactant concentration [C] used in the experiments. $[C]_{effective}$ is the concentration of surfactant monomers at the temperature of 275 K used for hydrate formation.

Surfactant	Weight (g/mol)	CMC[a] (mol m^{-3})	Krafft point (K)	[C][a] (mol m^{-3})	$[C]_{effective}$[a] (mol m^{-3})
SC_8S	232.3	140 (32500)	< 275	10.4 (2416)	10.4 (2416)
$SC_{10}S$	260.3	33 (8600)	280	10.4 (2707)	10.4 (2707)
$SC_{11}S$	274.4	16 (4390)	284	10.4 (2855)	10.4 (2855)
$SC_{12}S$	288.4	8.2 (2365)	289	10.4 (3000)	7.63[b] (2200)
$SC_{13}S$	302.4	4.3 (1300)	303	10.4 (3145)	2.76[c] (835)
$SC_{14}S$	316.4	2.1 (665)	311	10.4 (3291)	0.98[b] (300)
$SC_{16}S$	344.5	0.58 (200)	317	10.4 (3583)	0.12[b] (40)
$SC_{18}S$	372.5	0.23 (86)	325	10.4 (3874)	0.02[c] (7.8)

[a] Concentration in ppm is given between brackets.
[b] From Watanabe et al. (2005b).
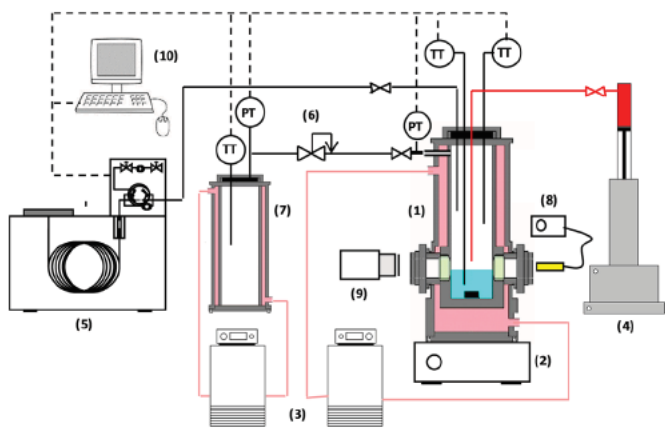[c] Calculated from Eq. (3).

Fig. 1. Schematic diagram of the experimental setup. (1) hydrate-formation cell; (2) magnetic agitator; (3) thermostatic baths; (4) syringe pump; (5) gas chromatograph; (6) pressure reducing valve; (7) gas storage vessel; (8) lighting system; (9) video camera; (10) data acquisition system.

became limpid. Before each increase in the bath temperature, the test tubes were moderately shaken. The Krafft point of a given surfactant was then defined as the temperature at which the precipitates were no longer visible to the naked eye. The un certainty of the measured T_k value is ± 1 K. Note that the Krafft point under gas hydrate formation conditions is known to be the same as the Krafft point at atmospheric pressure (Zhang et al., 2007a, 2007b).

2.3. Hydrate formation

The setup used for the hydrate formation experiment is sche matically depicted in Fig. 1. The hydrate formation cell is a jacketed cylindrical vessel made of stainless steel with an internal volume, V_{cell} of 364.7 ± 0.9 cm^3. It has two sapphire windows of 20 mm in diameter and a star shaped magnetic agitator for stir ring. A jacketed gas storage vessel and a high pressure syringe pump (ISCO 100 DM) are used respectively to load the gas mixture and inject the THF into the cell.

A gas chromatograph (Agilent, Model GC6890), connected to the cell, is used to sample and analyze the gas phase composition. The gas and liquid temperatures in the cell are measured using PT100 probes with an accuracy of ± 0.2 K, and the cell pressure is measured with a 0 10 MPa pressure transducer accurate to within ± 0.02 MPa. The pressure and temperatures are recorded every second by a computer running an in house LabView® program. Throughout the experiments, the hydrate crystallization is

observed and recorded by means of a CCD camera connected to a computer. For a hydrate formation experiment, the cell is loaded with $V_{sol} = 65.0 \pm 0.1$ cm^3 of the surfactant solution, purged twice with the gas phase to remove the air remaining in the system, and then pressurized to P_0 at $T_0 = 293$ K. P_0 was set to 3.5 MPa, 4.0 MPa, 4.8 MPa and 5.6 MPa for the CO$_2$, the 75:25 and 25:75 gas mix tures, and the CH$_4$ respectively. These pressure and temperature conditions are outside the stability zone of the hydrates formed with these gases. The surfactant solution in the cell reaches half way up the sapphire windows, and the tip of the tubing used for THF injection is located in the gas phase, a few millimeters above the w/g interface. The agitator is started and set to 600 rpm, and the cell is cooled at a rate of 0.9 K/min to T_{targ} (275 K). One hour after the pressure has reached a constant value (2.8 MPa, 3.4 MPa, 4.3 MPa and 5.1 MPa for the CO$_2$, the 75:25 and 25:75 gas mix tures, and the CH$_4$ respectively) at T_{targ}, the agitator is stopped (the hydrate formation experiment is thus conducted under *quiescent conditions*) and 0.30 ± 0.01 cm^3 of THF is injected in one shot, at the rate of 10 cm^3/min, with the syringe pump (Ricaurte et al., 2014c). As suggested by results presented in previous studies (Ricaurte et al., 2013; Ricaurte et al., 2014c), the amount of THF injected (0.4 wt% of the aqueous phase) is too low to significantly affect hydrate formation. In the experiments presented below, in which the surfactants effectively promoted hydrate formation, the amount of mixed hydrate containing THF (with the assumption that all the THF molecules participated to hydrate formation) is estimated to be lower than 3.5% of the hydrates formed. The cell temperature is maintained at T_{targ} until pressure stabilizes. Note that the subcooling, which is initially of about 5 K for all systems, continuously varies throughout the hydrate formation process (due to the batch type operations performed here), and eventually decreases to 0 K for the systems for which cell pressure has reached the three phase (L$_w$ H V) equilibrium pressure when hydrate formation has ceased at T_{targ}. Finally, the cell temperature is raised to T_0 at a rate of 1.5 K/min.

3. Results and discussion

3.1. Hydrate formation behavior

The typical variation in cell pressure and cell temperature ob served in the presence of a surfactant that promotes hydrate for mation is shown in Fig. 2a. In this example, the surfactant was SC$_{12}$S, and the gas phase was the 75:25 gas mixture. From point A to B, the cell is cooled from T_0 to T_{targ}. The decrease in cell pressure resulting from this variation in temperature is caused by both the

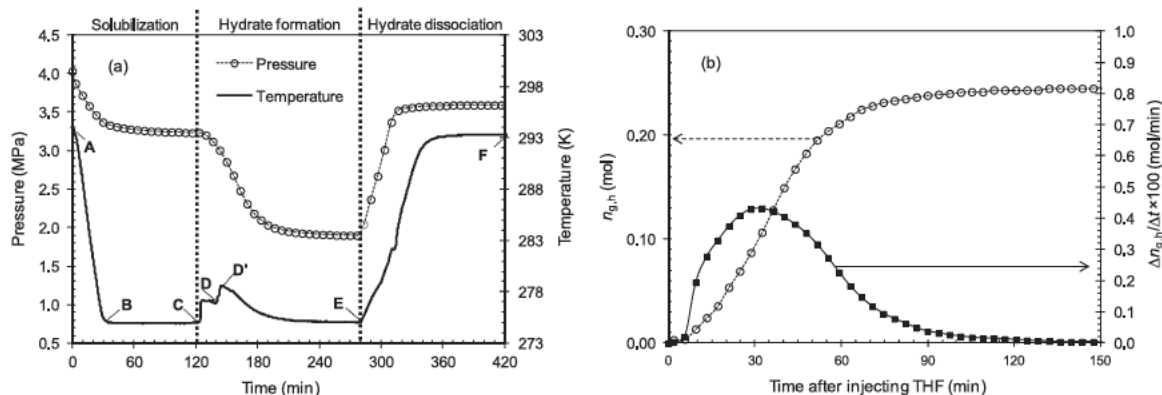**Fig. 2.** Typical pressure and temperature variations during an hydrate formation experiment: (a) cell pressure and cell temperature as a function of time; (b) mole number of gas enclathrated and gas enclathration rate as a function of time. Gas phase: 75 mol% CO$_2$ and 25 mol% CH$_4$. Initial pressure P_0 4 MPa, initial temperature T_0 293 K, and hydrate formation temperature T_{targ} 275 K.

contraction and solubilization of the gases (mainly CO_2 for the latter) in the $SC_{12}S$ solution. Approx. one hour after the pressure in the cell has stabilized, THF is injected into the surfactant solution. The injection causes — generally a few dozen seconds later — the onset of hydrate crystallization (first rise of the cell temperature at point C in Fig. 2a). A few minutes later (point D), a second increase in the cell temperature is observed. In all probability, the transient THF supersaturation produced at the injection point triggers the formation of a first hydrate, doubtless a mixed hydrate containing THF, CO_2 and CH_4 in the present case, which then acts as seeds for the formation of the CO_2–CH_4 binary hydrate. The steep decrease in cell pressure observed after point D′ reflects the formation of a large amount of hydrate. Cell pressure decreases until the three phase (L_W–H–V) equilibrium pressure is reached (point E). The cell is then heated from T_{targ} to T_0 to decompose the hydrates formed.

Fig. 2b shows the mole number of the gas enclathrated in the hydrate phase $n_{g,h}$ and the gas enclathration rate $\Delta n_{g,h}/\Delta t$ as a function of time, with $t=0$ min corresponding to the THF injection point. We used $\Delta t = 3.40$ min for all experiments.

$n_{g,h}$ is calculated using (Eqs. (1) and 2):

$$n_{g,h}(t) \approx n_{g,rv}(t) = \sum_i n_{i,rv}(t) \qquad (1)$$

with $n_{i,rv} = n_{i,v}(0) - n_{i,v}(t) = \left.\dfrac{y^i PV}{zRT}\right|_{t=0} - \left.\dfrac{y^i PV}{zRT}\right|_{t}$ (2)

where $i = CO_2$ or CH_4, and the subscripts "rv", "v" and "h" mean "removed from the vapor phase", "vapor phase", and "hydrate phase" respectively. P, T, V, z and R denote the cell pressure, the cell temperature, the gas phase volume, the compressibility factor, and the gas constant respectively. z is calculated using the Peng Robinson equation of state.

The change in V resulting from the expanding of liquid water volume during the hydrate formation was not taken into account. Then, V is taken to be constant at 299.7 cm^3 ($= V_{cell} - V_{sol}$) in Eq.2.

The hydrate phase that is forming starts to consume the gas a few minutes later the THF injection, and $\Delta n_{g,h}/\Delta t$ reaches a maximum value $(\Delta n_{g,h}/\Delta t)_{Max}$ about 30 min later, before decreasing to almost zero about 100 min after the peak. Note that the maximum value of the enclathration rate was not observed at the temperature spike (point D′ in Fig. 2a) but a few minutes later (12 min in the example given in Fig. 2).

In the cases where no surfactants were present or the surfactants did not promote hydrate growth, a single peak in the profile of the cell temperature and no significant gas consumption were observed after the THF injection.

It is worth noting that the surfactant concentration of 10.4 $mol\ m^{-3}$ is higher than the CMC of the surfactants that have more than 11 carbon atoms in their alkyl chain (Table 1). Because their Krafft points are higher than T_{targ}, these surfactants are consequently in a crystalline form. This can be clearly observed in the snapshots of the systems taken at T_{targ} a few minutes before hydrate formation (Fig. 3). The aqueous phases containing a surfactant with more than 11 carbon atoms are turbid.

The solubility C_s beyond which the surfactant molecules form a hydrated solid in an aqueous solution at 275 K is reported to be 7.63 $mol\ m^{-3}$, 0.98 $mol\ m^{-3}$ and 0.12 $mol\ m^{-3}$ for $SC_{12}S$, $SC_{14}S$ and $SC_{16}S$ respectively (Watanabe et al., 2005b). Based on the empirical Eq. (3) below, deduced by fitting the experimental solubility points above, the solubility of $SC_{13}S$ and $SC_{18}S$ is estimated to be 2.76 $mol\ m^{-3}$ and 0.02 $mol\ m^{-3}$, respectively.

$$C_s = 2.10^6 \exp(-1.038x) \qquad (3)$$

where x is the number of carbon atoms of the surfactant alkyl chain.

The concentration of surfactant monomers at T_{targ} is therefore much lower for surfactants $SC_{12}S$ to $SC_{18}S$ than for the other ones used (see $[C]_{effective}$ in Table 1).

The hydrate formation observed through the sapphire windows of the cell reveals very different behavior depending on whether a surfactant is present. In the absence of SC_xS, a hydrate crust forms at the w/g interface (see the snapshots labeled "WS" in Fig. 4). The crust grows slightly downward (below the w/g interface) and becomes a few millimeters thick a couple of minutes after the onset of hydrate crystallization. In the presence of SC_xS, the hydrate phase expands upwards and downwards of the w/g interface, to tally covering the sapphire windows within a few minutes. This formation behavior has been observed to occur for all the surfactants tested. However, as we will see in the next paragraph, the rate of hydrate formation and the amount of hydrate formed are dependent on both the surfactant carbon chain length and the gas phase composition.

3.2. Effect of the surfactant carbon chain length and gas phase composition

The values of the total mole number of the gas enclathrated in the hydrate phase, $(n_{g,h})_{Tot}$ and the maximum gas enclathration rate, $(\Delta n_{g,h}/\Delta t)_{Max}$ obtained for the surfactant series and the different gas phase compositions studied are given in Table 2 and plotted in Fig. 5. Some of the experiments were duplicated in order to evaluate their reproducibility, and the relative dispersion of $(n_{g,h})_{Tot}$ and $(\Delta n_{g,h}/\Delta t)_{Max}$ values was generally found to be lower
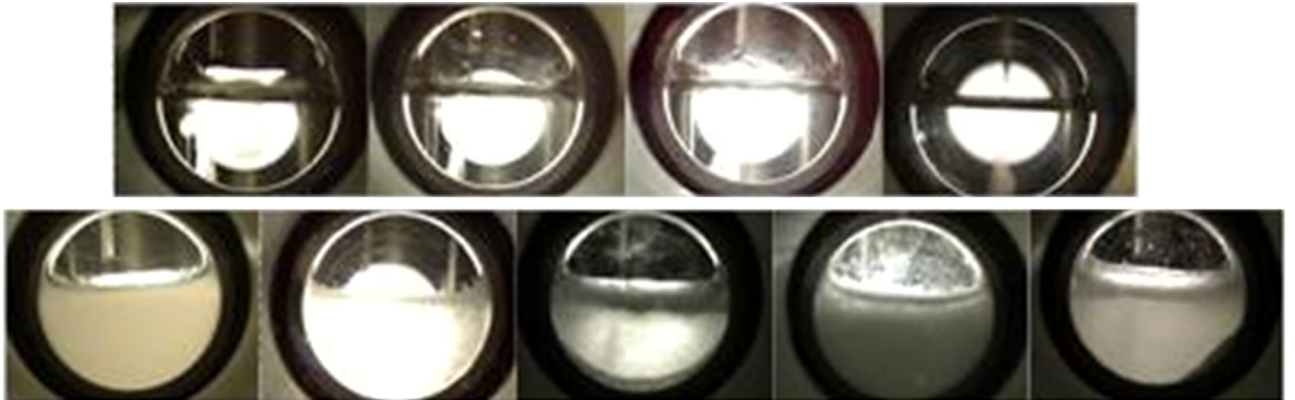

Fig. 3. Snapshots of the systems containing 10.4 $mol\ m^{-3}$ of SC_xS at T_{targ} 275 K. Upper part, from the left to the right: system without surfactant, and systems with SC_xS with x 8, 10 and 11. Lower part, from the left to the right: systems with SC_xS with x 12, 13, 14, 16 and 18. Gas phase: 75 mol% CO_2 and 25 mol% CH_4. Pressure P 3.4 MPa.
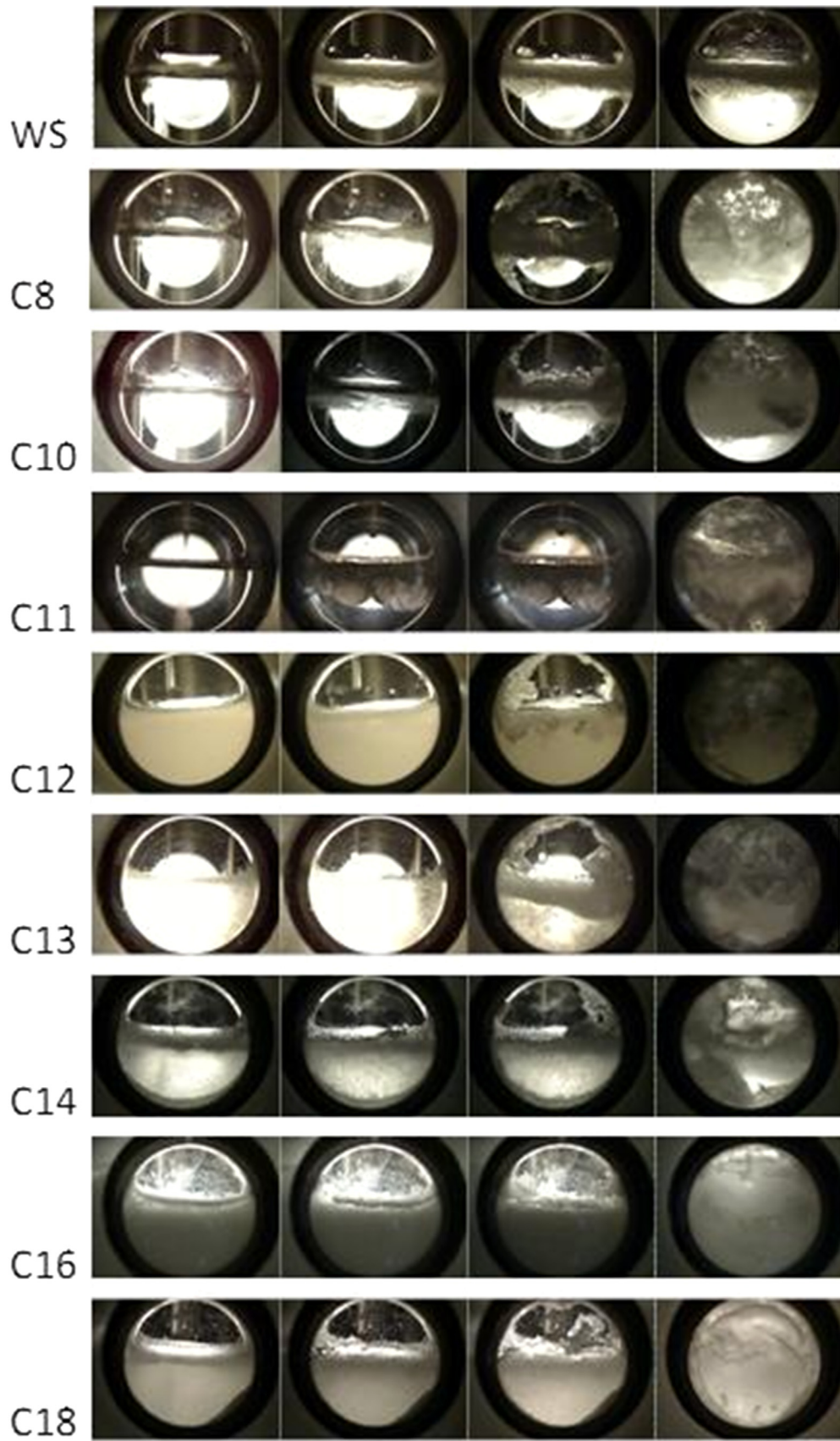
Fig. 4. Snapshots of the systems without surfactant (WS) or with 10.4 mol.m^{-3} of SC$_x$S (with $x = 8$ to 18) at $T_{\text{targ}} = 275$ K. The snapshots were taken at $t = 0$, 20, 60 and 600 s after injecting THF. Gas phase: 75 mol% CO_2 and 25 mol% CH_4. Initial pressure $P_0 = 4$ MPa.

Table 2
Total mol number (mmol) of gas enclathrated in the hydrate phase and maximum gas enclathration rate (between brackets, mmol min^{-1}) for the different surfactants and gas phases used in this work. The dash corresponds to experiment which was not performed.

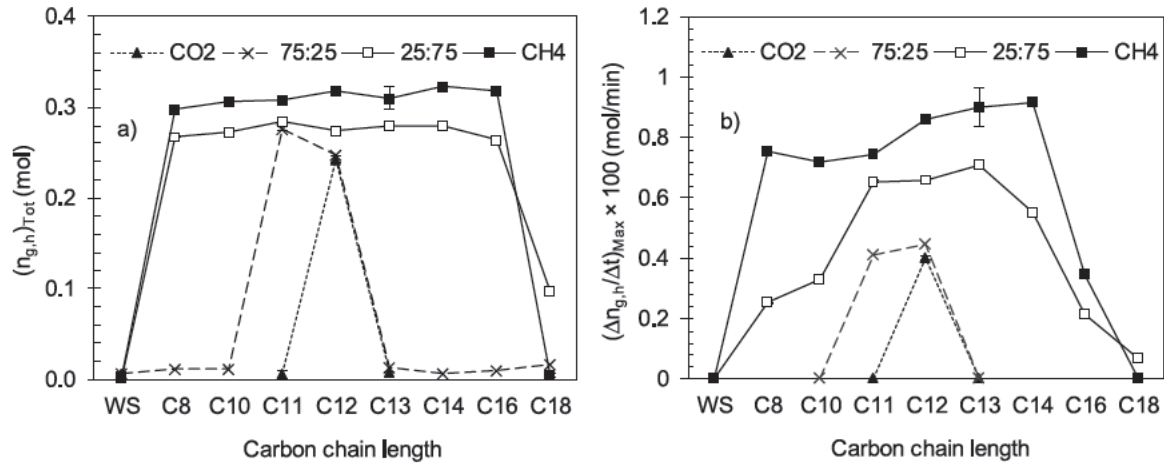| System	WS	SC$_8$S	SC$_{10}$S	SC$_{11}$S	SC$_{12}$S	SC$_{13}$S	SC$_{14}$S	SC$_{16}$S	SC$_{18}$S
CO$_2$	6.8 (~0)	–	–	6.3 (~0)	245.4 (3.93)	8.9 (~0)	–	–	–
75%CO$_2$:25%CH$_4$	6.7 (~0)	11.2 (~0)	12.2 (~0)	276.2 (4.09)	246.4 (4.48)	13.3 (~0)	5.9 (~0)	9.7 (~0)	16.2 (~0)
25%CO$_2$:75%CH$_4$	1.8 (~0)	267.7 (2.51)	272.9 (3.28)	283.7 (6.55)	273.4 (6.60)	278.9 (7.09)	279.1 (5.54)	263.8 (2.14)	97.8 (0.69)
CH$_4$	3.4 (~0)	297.5 (7.57)	305.7 (7.21)	308.2 (7.45)	318.1 (8.62)	323.5 (9.00)	322.4 (9.15)	317.6 (3.46)	5.3 (~0)

Fig. 5. a) Total mole number of gas enclathrated in the hydrate phase and b) maximum gas enclathration rate as a function of surfactant carbon chain length and gas-phase composition. The lines are only visual guides. Initial pressure P_0 5.6, 4.8, 4.0, and 3.5 MPa for the system with pure CH$_4$, 25:75, 75:25 and pure CO$_2$, respectively. Initial temperature T_0 293 K, and hydrate formation temperature T_{targ} 275 K.

than 1% (and in all cases lower than 10%).

In the systems without surfactant, the hydrate crust that formed at the w/g interface appeared to rapidly impede contact between the water and gas phases, stopping hydrate growth. Therefore, $(n_{g,h})_{Tot}$ is low and $(\Delta n_{g,h}/\Delta t)_{Max}$ is almost zero for all the gas phase compositions used. In the presence of surfactant, the values obtained for $(n_{g,h})_{Tot}$ and $(\Delta n_{g,h}/\Delta t)_{Max}$ depend on both the surfactant carbon chain length (noted below C$_x$) and the gas phase composition. In the case of the pure CH$_4$ and the 25:75 gas mixture, all the surfactants tested, except SC$_{18}$S, promoted hydrate growth. However, the C$_x$ impacts $(n_{g,h})_{Tot}$ and $(\Delta n_{g,h}/\Delta t)_{Max}$ differently. On the one hand, $(n_{g,h})_{Tot}$ is fairly constant – with the exception of the system containing SC$_{18}$S – for both gas phase compositions (Fig. 5a). On the other hand, in the case of pure CH$_4$, $(\Delta n_{g,h}/\Delta t)_{Max}$ is fairly constant (and even appears to increase slightly with C$_x$) for the surfactant with up to 14 carbon atoms before dropping to a much smaller value for a longer C$_x$, whereas the 25:75 gas mixture $(\Delta n_{g,h}/\Delta t)_{Max}$ displays a bell shaped dependence on C$_x$ with a maximum value for the surfactants containing 11 to 13 carbon atoms in their alkyl chain (Fig. 5b). Despite there being fewer solubilized molecules at T_{targ} (see [C]$_{effective}$ in Table 1), the surfactants with 12 to 16 carbon atoms are just as effective (in terms of the amount of hydrate formed) as those with shorter C$_x$. Moreover, the surfactants with 14 and 16 carbon atoms showed low foaming tendency in comparison to those with shorter carbon chain length (see SI 1 in the Supplementary Material). This property could be very advantageous in practice if such additives were used in a hydrate based process. The above results on the promotion capacity of the surfactant depending on their alkyl chain length are consistent with those reported by Okutani et al. (2008) for pure CH$_4$ hydrate formed in a quiescent system at 275 K, which show that SC$_{12}$S, SC$_{14}$S and SC$_{16}$S lead to almost the same water to hydrate conversion ratio, and that SC$_{16}$S was less effective in increasing the hydrate growth rate than SC$_{12}$S and SC$_{14}$S.

For the 75:25 gas mixture, only the systems with SC$_{11}$S and SC$_{12}$S effectively produced hydrates (whereas the reaction quickly stopped with the other surfactants), and in the case of pure CO$_2$, only the one with SC$_{12}$S did. The latter result seems consistent with that reported by Jia et al. (2016) for pure CO$_2$ hydrate formed under unstirred condition at the same temperature as used in the present work, which shows that SC$_{12}$S has an efficient promotion effect on hydrate formation, while no obvious effect is observed when SC$_{18}$S is used.

For each experiment with SC$_{12}$S, which was the only surfactant of the series studied that promotes hydrate growth for all the gas phase compositions used, the water to hydrate conversion ratio, τ_{H_2O} was estimated using Eq. (4):

$$\tau_{H_2O} = \frac{N_h \cdot (n_{g,h})_{Tot}}{n_w} \qquad (4)$$

where N_h is the hydration number calculated with the CSMGem software program (Sloan and Koh, 2008) for the system studied at T_{targ}, and n_w is the mole number of water initially present in the solution with which the hydrate formation cell was charged. In every experiment, $n_w = 3.61$ mol.

The calculated values of τ_{H_2O} are listed in Table 3.

Table 3
Estimated water-to-hydrate conversion ratio, τ_{H_2O} obtained in the presence of SC$_{12}$S for the different gas-phase compositions used in this work. The hydration number, N_h and the theoretical equilibrium pressure, $P_{eq,th}$ have been calculated with the CSMGem software program. $(n_{g,h})_{Tot}$ and $(\Delta n_{g,h}/\Delta t)_{Max}$ have been extracted from Table 2. $P_{f,exp}$ is the pressure measured at the end of hydrate formation (point E in Fig. 2a).

CO$_2$:CH$_4$ ratio (mol%/mol%)	N_h	τ_{H_2O} (%)	$(n_{g,h})_{Tot}$ (mmol)	$(\Delta n_{g,h}/\Delta t)_{Max}$ (mmol/min)	$P_{f,exp}$ (MPa)	$P_{eq,th}$ (MPa)
100:0	6.7	45.5	245.4	3.93	1.56	1.57
75:25	6.5	44.4	246.4	4.48	1.80	1.73
25:75	6.3	47.7	273.4	6.60	2.60	2.44
0:100	6.3	55.5	318.1	8.62	3.16	3.17

Between 44% and 56% of the water molecules present in the system were converted to hydrate. These values are significantly lower than those obtained in other studies (Pang et al., 2007; Okutani et al., 2008). This is ascribable to the difference in the type of operations used to form hydrate. In batch type operations with excess water (as in our work), hydrate formation may go on until cell pressure has reached the three phase (L_w H V) equilibrium pressure at the experiment temperature (see the values of $P_{f,exp}$ and $P_{eq,th}$ at T_{targ} in Table 3). In semi continuous type operations (as in the experiments of Pang et al. (2007), and Okutani et al. (2008)), the system pressure is held constant and thus hydrate may form until no water is left for conversion.

Although the amount of water converted to hydrate was roughly the same for all the experiments performed with $SC_{12}S$, the effect of this surfactant on hydrate growth rate drastically diminished with the increase in the initial CO_2 fraction in the gas phase. The $(\Delta n_{g,h}/\Delta t)_{Max}$ value drops from 8.62 mmol/min for pure CH_4 to 3.93 mmol/min for pure CO_2.

Such a decrease might be due to the lower starting pressure (2.8 MPa) used in the experiment with pure CO_2 as compared to the higher starting pressure (5.1 MPa) available for pure CH_4 despite the same initial subcooling of about 5 K. Variations in the pressure driving force (difference between the starting pressure and the equilibrium pressure, at the experiment temperature (275 K in our case)) produce less effect on the driving force for hydrate formation than variations in the subcooling (see SI 2 in the Supplementary Material). Therefore, we do believe that the values of the hydrate formation rate obtained in these experiments are fairly representative of the intrinsic effect of the surfactant on the hydrate formation rate.

This decrease results from a change in hydrate formation behavior as the initial CO_2 fraction in the gas phase increases (Fig. 6). In the system with pure CH_4 (Fig. 6a), the w/g interface remained relatively free of hydrate several dozen seconds after the onset of hydrate crystallization. The hydrate crystals visible in the liquid layer below the w/g interface clustered in seemingly loose aggregates. Some small hydrate aggregates were observed to be carried along by strong streams oriented in the direction of the lateral walls of the sapphire windows (red arrows in the snapshot in Fig. 6a). The presence of these streams suggests that the growing hydrate phase formed a porous structure, which exerted a strong capillary suction on the "free water". Their direction proves that the porous hydrate structure grows on the sidewall of the reactor cell above the initial w/g interface, and, through the sapphire windows, the level of the w/g interface was observed to drop as the hydrate growth proceeded.

Almost same hydrate formation behavior was observed for the 25:75 gas mixture (Fig. 6b).

For the 75:25 gas mixture and for pure CO_2 (Fig. 6c and d), the w/g interface was totally covered by hydrate particles within a few seconds after the onset of hydrate crystallization. The hydrate crystals seem smaller and the aggregates more compact than those formed with pure CH_4 and the 25:75 gas mixture. They

(especially those formed with pure CO_2) propagated far more slowly on the sidewall of the cell. No drop in the level of water in the cell was observed, suggesting that the porous hydrate structure did not propagate much on the cell's sidewall above the initial w/g interface.

In order to obtain better insight into the effect of the initial CO_2 fraction in the CO_2/CH_4 gas phase on the hydrate formation behavior in the presence of $SC_{12}S$, we conducted a series of experiments in which hydrate formation was triggered at the top of a sessile $SC_{12}S$ solution drop by contact with a piece of gas hydrate (formed from the same solution) hanging at the tip of a stainless steel capillary. Details on the apparatus and experimental procedure used can be found in a recent article by Daniel David et al. (2015). In our experiments, cell pressure and cell temperature were the same as those reached by the system just before the THF injection in the experiments conducted in the reactor cell, namely $P=2.8$ MPa, 3.4 MPa, 4.3 MPa and 5.1 MPa for the CO_2, the 75:25 and 25:75 gas mixtures, and the CH_4 respectively, and $T=T_{targ}$ ($=275$ K). The $SC_{12}S$ concentration was 10.4 mol m^{-3}.

As in the study of Daniel David et al. (2015), we observed two different growth patterns. One for the systems with pure CH_4 and the 25:75 gas mixture, and the other for those with pure CO_2 and the 75:25 gas mixture. In the former case (snapshots a) and b) in Fig. 7), the hydrate that crystallized at the tip of the stainless steel capillary spread over it forming a thick porous hydrate layer. When this hanging hydrate was brought into contact with the sessile liquid drop, the drop was very rapidly, and almost totally, sucked up by the hydrate phase (see the M1 and M2 videos in the Supplementary Material) where it was converted to hydrate. In the latter case (snapshots c) and d) in Fig. 7), the hydrate porous layer formed on the stainless steel capillary appeared much thinner, and when the hanging hydrate was brought into contact with the sessile liquid drop, the drop was not sucked up but converted to hydrate directly on its support (see the M3 and M4 videos in the Supplementary material). The main difference between our observations and Daniel David's is that, in our experiments with pure CO_2 and the 75:25 gas mixture, the sessile liquid drop was apparently totally converted to hydrate (small hydrate particles dispersed over the support were visible at the end of hydrate formation), whereas some liquid water (not converted to hydrate) remained in the core of the sessile drop in their experiments. The higher water to hydrate conversion rate we obtained is certainly due to the much higher $SC_{12}S$ concentration we used (6 to 30 times those used by Daniel David et al. (2015)).

From these experiments, we can infer that the CH_4 and 25:75 gas hydrates produced from the 10.4 mol m^{-3} $SC_{12}S$ solution form a porous structure with a very high water wettability, which wets the stainless steel capillary. The water wettability of the hydrate porous structure formed drastically decreases when CO_2 is the dominant specie in the gas phase, and the capacity of this hydrate to wet the stainless steel capillary also seems to decrease.

The differences observed in the hydrate formation behavior certainly result from differences in the adsorption behavior of the
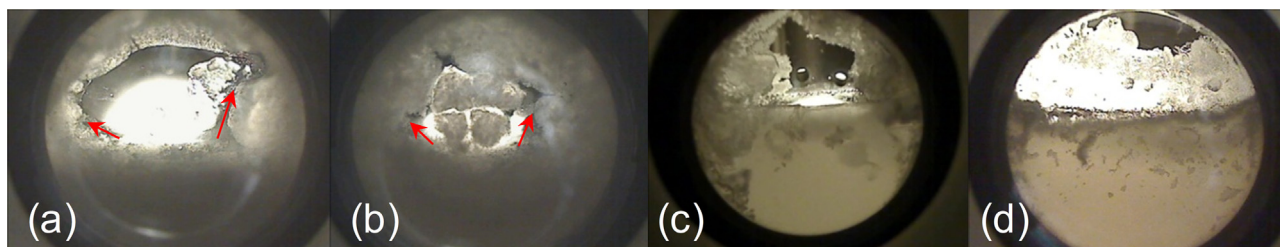

Fig. 6. Snapshots of hydrate formation for the systems containing a 10.4 mol m^{-3} $SC_{12}S$ solution and different gas phases, at T_{targ} 275 K. The gas phases and pressures are: (a) pure CH_4, 5.1 MPa, (b) 25 mol% CO_2:75 mol% CH_4, 4.3 MPa, (c) 75 mol% CO_2:25 mol% CH_4, 3.4 MPa, and (d) pure CO_2, 2.8 MPa. The snapshots were taken 50 s after the beginning of hydrate crystallization. The red arrows show the direction of streams observed in the $SC_{12}S$ solution.
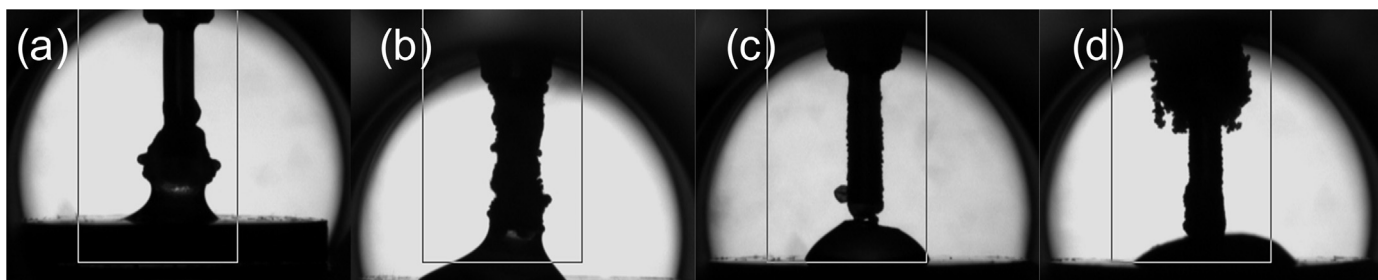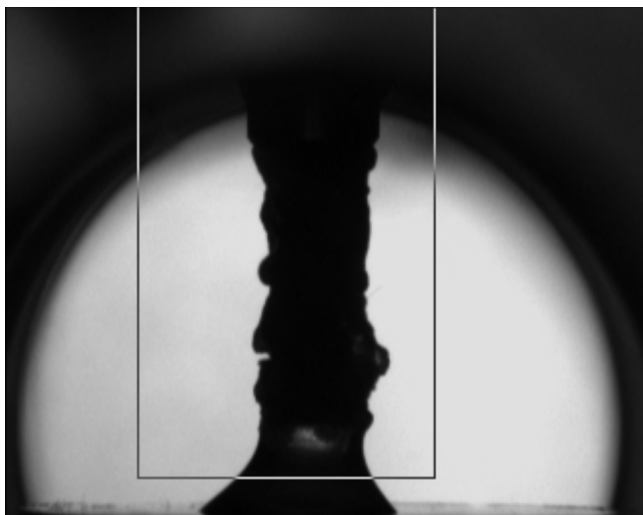
Fig. 7. Snapshots of hydrate growth for the systems containing 10.4 mol m^{-3} of SC$_{12}$S and different gas phases, at T_{targ} 275 K. The hanging hydrate is made from the same SC$_{12}$S solution. The gas phases and pressure are: (a) pure CH$_4$, 5.1 MPa, (b) 25 mol% CO$_2$:75 mol% CH$_4$, 4.3 MPa, (c) 75 mol% CO$_2$:25 mol% CH$_4$, 3.4 MPa, and (d) pure CO$_2$, 2.8 MPa.

Video 1. M1 video. View at the millimetric scale of the hydrate growth pattern for the system containing a 10.4 mol m^{-3} SC$_{12}$S solution and pure CH$_4$, at T 275 K and P 5.1 MPa. A hanging hydrate, is brought into contact with a sessile liquid drop. A video clip is available online.Supplementary material related to this article can be found online at http://dx.doi.org/10.1016/j.ces.2016.06.034.
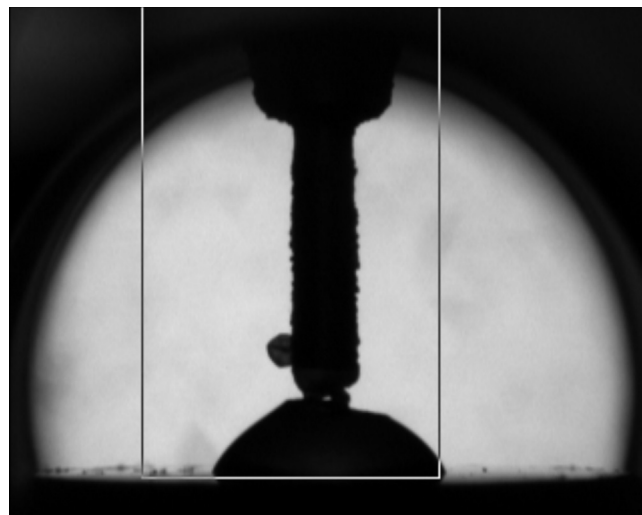
Video 3. M3 video. View at the millimetric scale of the hydrate growth pattern for the system containing a 10.4 mol m^{-3} SC$_{12}$S solution and the 75:25 gas mixture, at T 275 K and P 3.4 MPa. A hanging hydrate, is brought into contact with a sessile liquid drop.Supplementary material related to this article can be found online at http://dx.doi.org/10.1016/j.ces.2016.06.034.
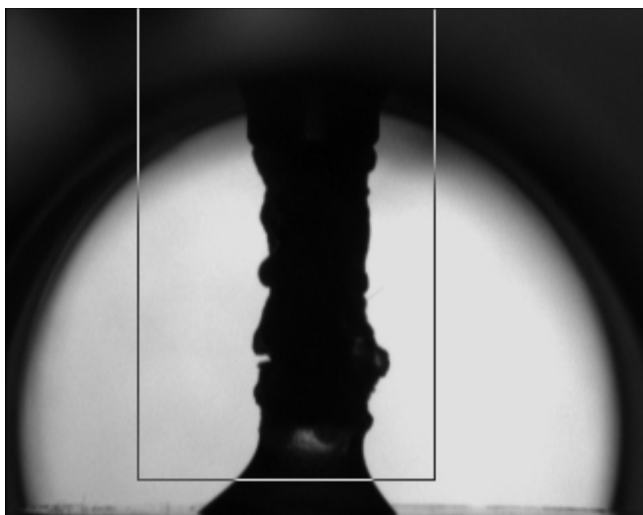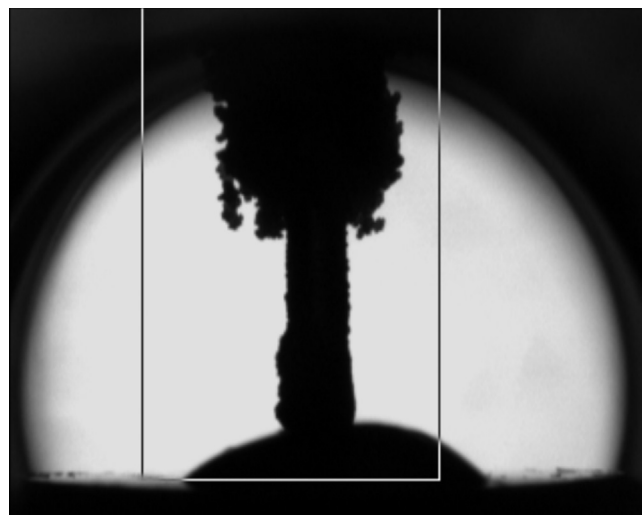

Video 2. M2 video. View at the millimetric scale of the hydrate growth pattern for the system containing a 10.4 mol m^{-3} SC$_{12}$S solution and the 25:75 gas mixture, at T 275 K and P 4.3 MPa. A hanging hydrate, is brought into contact with a sessile liquid drop.Supplementary material related to this article can be found online at http://dx.doi.org/10.1016/j.ces.2016.06.034.

Video 4. M4 video. View at the millimetric scale of the hydrate growth pattern for the system containing a 10.4 mol m^{-3} SC$_{12}$S solution and pure CO$_2$, at T 275 K and P 2.8 MPa. A hanging hydrate, is brought into contact with a sessile liquid drop. Supplementary material related to this article can be found online at http://dx.doi.org/10.1016/j.ces.2016.06.034.

C$_{12}$S$^-$ anions both onto the hydrate surface and onto the sidewalls of the hydrate formation cell, depending on the initial CO$_2$ fraction in the gas phase. In a study on the adsorption of C$_{12}$S$^-$ on THF

hydrate based on pyrene fluorescence measurements, Zhang et al. (2010) showed that the presence of carbonate reduces the ad sorption density of C$_{12}$S$^-$ on hydrates. Because the pH of the water

phase at the pressure and temperature at which CO_2 hydrate forms is around 3 which implies that the dominant *ionic* species is bicarbonate (HCO_3^-) not carbonate they concluded that the competitive adsorption between HCO_3^- and $C_{12}S^-$ might be responsible for the moderate promotion effect of $SC_{12}S$ in the case of the CO_2 hydrate as compared to other hydrates. The same competitive adsorption between $C_{12}S^-$ and HCO_3^- probably also occurs at the surface of the stainless steel sidewalls of the cell, which under acidic pH conditions, is positively charged (stainless steel has a point of zero charge of ~ 8.5 (Takahashi and Fukuzaki, 2008)). In our experiments, this competitive adsorption seems to become more and more favorable to $C_{12}S^-$ as the $CO_2:CH_4$ ratio in the gas mixture, and the resulting bicarbonate concentration in the aqueous phase, decreases, causing the observed increase in $(\Delta n_{g,h}/\Delta t)_{Max}$. The decrease in the acceleration effect of $SC_{12}S$ observed for the high initial CO_2 fractions in the gas phase might also result from a distortion of the $SC_{12}S$ molecular geometry induced by its interaction with CO_2. Alberti et al. (2013) demonstrated using molecular dynamics calculations that, in the presence of CO_2 molecules, the shape of the $SC_{12}S$ molecule changes ("it folds to form a kind of helix") but this deformation does not happen in the presence of CH_4 molecules (Alberti et al., 2012). Their MD calculations showed that the distortion of $SC_{12}S$ molecular geometry hinders the formation of clathrate like structures from CO_2 water clusters. In the absence of molecular deformation, $SC_{12}S$ was found to have a structuring effect on the water molecules favorable to the formation of a clathrate hydrate structure. The latter point has also been supported by spectral data obtained on CP hydrate with $C_{12}S^-$ adsorbed on its surface (Lo et al., 2012).

All the observations we made throughout the experiments demonstrate that for gas hydrates to form rapidly and in large quantities from a liquid solution and pure or mixed CO_2/CH_4 gases, and under quiescent conditions, the capillarity driven mechanism must be able to develop efficiently. This will occur if the surfactant used is conducive to the formation of a water wettable porous hydrate structure, which is able to grow on the sidewalls of the hydrate formation cell. The capacity of the surfactant molecules to be readily adsorbed onto the hydrate surface and to prevent the hydrate particles from agglomerating into a compact, non porous hydrate structure is certainly pivotal to efficient hydrate formation. For agglomeration not to occur, the hydrate particles need to be rapidly coated with sufficient surfactant molecules. In addition, the adsorbed surfactant layer must maintain high wettability for the hydrate particles, meaning the hydrophilic group of the adsorbed surfactant molecules must be predominantly oriented away from the hydrate surface. At the surfactant concentration used in the present work, $C_{12}S^-$ anions might first be adsorbed via hydrogen bonds onto the hydrate surface in a head down configuration (Lo et al., 2008), after which further adsorption would occur via mutual attraction of the hydrophobic chains of oncoming $C_{12}S^-$ and those of previously adsorbed $C_{12}S^-$. The surfactant aggregates (or hemimicelles) thus formed on the hydrate surface would make the hydrate particles more wettable by the aqueous solution, and the electrostatic repulsion between the adsorbed surfactant aggregates would limit (or prevent) agglomeration of the hydrate particles (Fig. 8). The same type of adsorption might occur on the surface of the stainless steel sidewalls of the cell.

Comparison of the $(\Delta n_{g,h}/\Delta t)_{Max}$ values obtained in our experiments clearly shows that the efficiency of the SC_xS surfactants does not vary monotonously with C_x, but reaches a maximum for C_x within a certain range (roughly between 11 and 14). The surfactants with a shorter carbon chain probably have a lower propensity to be adsorbed onto the hydrate surface due to their higher solubility in bulk water. The lower mutual attraction of their (short) hydrophobic groups might also render hemimicelle formation more difficult. Those with a longer carbon chain should be
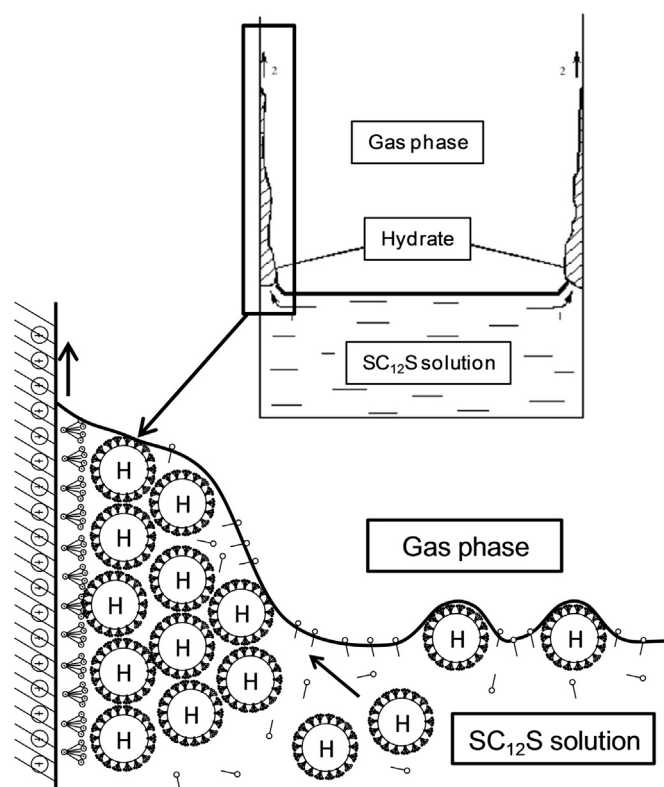

Fig. 8. Schematic representation of $C_{12}S^-$ adsorption onto the CH_4/CO_2 hydrate surface and the surface of the stainless steel sidewalls of the hydrate-formation cell, and agglomeration of the hydrate particles into a porous structure.

adsorbed and form hemimicelles on the hydrate surface more readily, because the mutual attraction of the hydrophobic groups increases with the length of the chain. However, due to the low concentration of the surfactant monomers in the water phase at T_{targ} (see Table 1) and the presumably slow kinetics of dissolution of the surfactant precipitates (Abdel Rahem and Al Hawarin, 2007), hemimicelles may not form on the growing hydrate surface at a sufficient speed to efficiently protect the hydrate particles from agglomeration. These limitations, which are presumably detrimental to efficient development of the capillarity driven mechanism, are expected to become even more prevalent as the amount of CO_2 in the system increases, since the surfactant molecule probably has to compete with bicarbonate to be adsorbed onto the hydrate surface. Moreover, the molecular geometry of the surfactant molecule might undergo a distortion making it less conducive to hydrate formation, and maybe to its adsorption onto the hydrate surface. These are possible explanation as to why the range of C_x that enables a high hydrate growth rate narrows when the $CO_2:CH_4$ ratio increases.

4. Conclusions

The experimental investigations performed in this study have shown that the effect of the carbon chain length of sodium alkyl sulfates on their capacity to promote hydrate growth in quiescent $CO_2/CH_4/$water systems strongly depends on the initial CO_2 fraction in the gas phase: the lower the fraction, the greater the promotion effect. Strong promotion of hydrate formation was observed to rely on efficient development of the capillarity driven mechanism, which means that a water wettable porous hydrate structure has to form and be able to spread over the inner sidewalls of the hydrate formation cell. For this to occur, the adsorbed

surfactant molecules must predominantly be oriented away from the hydrate surface. For hydrate formed with pure CH_4, the capillarity driven mechanism develops efficiently for surfactants with a number of carbon atoms in their hydrophobic chain ranging from 8 14. The more the CO_2:CH_4 ratio increases, the narrower the range becomes, and with pure CO_2, the only surfactant that effectively promotes hydrate formation contains 12 carbon atoms. Competitive adsorption between C_xS and bicarbonate is probably responsible for the decrease in the surfactant efficiency observed as the CO_2 fraction in the initial gas phase increases.

Appendix A. Supplementary material

Supplementary data associated with this article can be found in the online version at http://dx.doi.org/10.1016/j.ces.2016.06.034.

References

Abdel-Rahem, R., Al-Hawarin, J., 2007. Dissolution rate of sodium fatty alcohol sulfate FAS-surfactants. J. Tenside Surfactants Deterg. 44 (5), 260–265.

Adeyemo, A., Kumar, R., Linga, P., Ripmeester, J., Englezos, P., 2010. Capture of carbon dioxide from flue or fuel gas mixtures by clathrate crystallization in a silica gel column. Int. J. Greenh. Gas Control 4, 478–485.

Alberti, M., Costantini, A., Lagana, A., Pirani, F., 2012. Are micelles needed to form methane hydrates in sodium dodecyl sulfate solutions? J. Phys. Chem. B 116, 4220–4227.

Alberti, M., Pirani, F., Lagana, A., 2013. Carbon dioxide clathrate hydrates: selective role of intermolecular interactions and action of SDS catalyst. J. Phys. Chem. A 117, 6991–7000.

Belosludov, V.R., Subbotin, O.S., Krupskii, D.S., Belosludov, R.V., Kawazoe, Y., Kudo, J. I., 2007. Physical and chemical properties of gas hydrates: theoretical aspects of energy storage application. Mater. Trans. 48 (4), 704–710.

Clain, P., Delahaye, A., Fournaison, L., Mayoufi, N., Dalmazzone, D., Fürst, W., 2012. Rheological properties of tetra-n-butylphosphonium bromide hydrate slurry flow. Chem. Eng. J. 193–194, 112–122.

Daimaru, T., Yamasaki, A., Yanagisawa, Y., 2007. Effect of surfactant carbon chain length on hydrate formation kinetics. J. Petrol. Sci. Eng. 56, 89–96.

Daniel-David, D., Guerton, F., Dicharry, C., Torré, J.-P, Broseta, D., 2015. Hydrate growth at the interface between water and pure or mixed CO_2/CH_4 gases: influence of pressure, temperature, gas composition and water-soluble surfactants. Chem. Eng. Sci. 132, 118–127.

Gayet, P., Dicharry, C., Marion, G., Graciaa, A., Lachaise, J., Nesterov, A., 2005. Experimental determination of methane hydrate equilibrium curve up to 55 MPa by using a small amount of surfactant as hydrate promoter. Chem. Eng. Sci. 60 (21), 5751–5758.

Gudmundsson, J.S., Andersson, V., Levik, O.I., Parlaktuna, M.M., 1999. Natural gas hydrates: a new gas transportation form. J. Petrol. Tech. 51 (4), 66–67.

Hanif, A, Suhartanto, T, Green, M.L.H., 2002. Possible utilisation of CO_2 on Natuna's gas field using dry reforming of methane to syngas (CO & H_2). In: Proceedings of SPE – Asia Pacific Oil and Gas Conference, Melbourne, Australia, pp. 833–840.

Jia, J.J, An, Y., Wang, F., Luo, S.J., Guo, R.B., 2016. Effect of anionic surfactants with different carbon chain lengths on CO_2 hydrate formation. In: Chen, P., (Ed.) Material Science and Environmental Engineering: Proceedings of ICMSEE2015, Wuhan, Hubei, China. CRC Press, Taylor and Francis Group, London, pp. 429–422.

Kang, S.-P., Lee, J.-W., 2010. Kinetic behaviors of CO_2 hydrates in porous media and

effect of kinetic promoter on the formation kinetics. Chem. Eng. Sci. 65, 1840–1845.

Kumar, A., Bhattacharjee, G., Kulkarni, B.D., Kumar, R., 2015. Role of surfactants in promoting gas hydrate formation. Ind. Eng. Chem. Res. . http://dx.doi.org/10.1021./acs.iecr.5b03476

Linga, P., Kumar, R., Lee, J.D., Ripmeester, J., Englezos, P., 2010. A new apparatus to enhance the rate of gas hydrate formation: application to capture of carbon dioxide. Int. J. Greenh. Gas Control 4, 630–637.

Lo, C., Zhang, J.S., Somasundaran, P., Lu, S., Couzis, A., Lee, J.W., 2008. Adsorption of surfactants on two different hydrates. Langmuir 24 (22), 12723–12726.

Lo, C., Zhang, J., Somasundaran, P., Lee, J.W., 2010. Raman spectroscopic studies of surfactant effect on the water structure around hydrate guest molecules. J. Phys. Chem. Lett. 1, 2676–2679.

Lo, C., Zhang, J., Somasundaran, P., Lee, J.W., 2012. Investigations of surfactant effects on gas hydrate formation via infrared spectroscopy. J. Colloids Interf. Sci. 376, 173–176.

Okutani, K., Kuwabara, Y., Mori, Y.H., 2008. Surfactant effects on hydrate formation in an unstirred gas/liquid system: an experimental study using methane and sodium alkyl sulfates. Chem. Eng. Sci. 63 (1), 183–194.

Pang, W.X., Chen, G.J., Dandekar, A., Sun, C.Y., Zhang, C.L., 2007. Experimental study on the scale-up effect of gas storage in the form of hydrate in a quiescent reactor. Chem. Eng. Sci. 62, 2198–2208.

Rasi, S., Veijanen, A., Rintala, J., 2007. Trace compounds of biogas from different biogas production plants. Energy 32 (8), 1375–1380.

Ricaurte, M., Dicharry, C., Broseta, D., Renaud, X., Torré, J.-P., 2013. CO_2 Removal from a $CO_2 - CH_4$ gas mixture by clathrate hydrate formation using THF and SDS as water-soluble hydrate promoters. Ind. Eng. Chem. Res. 52, 899–910.

Ricaurte, M., Dicharry, C., Renaud, X., Torré, J.-P., 2014a. Combination of surfactants and organic compounds for boosting CO_2 separation from natural gas by clathrate hydrate formation. Fuel 122, 206–217.

Ricaurte, M., Torré, J.-P., Diaz, J., Dicharry, C., 2014b. Effect of the concentration and carbon chain length of sulfate-based surfactant on hydrate formation kinetics. In: Proceedings of the 8th International Conference on Gas Hydrates, Bejing, China, T1-152.

Ricaurte, M., Torré, J.-P., Diaz, J., Dicharry, C., 2014c. In situ injection of THF to trigger gas hydrate crystallization: application to the evaluation of a kinetic hydrate promoter. Chem. Eng. Res. Des. 92 (9), 1674–1680.

Rosen, M.J., Kunjappu, J.T., 2012. Surfactants and Interfacial Phenomena, 4th ed. Wiley, New Jersey.

Sloan, E.D., Koh, C.A., 2008. Clathrate Hydrates of Natural Gases, 3rd ed. CRC Press, Boca Raton.

Takahashi, K., Fukuzaki, S., 2008. Cleanability of titanium and stainless steel particles in relation to surface charge aspects. Biocontrol Sci. 13 (1), 9–16.

Wang, F., Jia, Z.-Z., Luo, S.-J., Fu, S.-F., Wang, L., Shi, X.-S., Wang, C.-S., Guo, R.-B., 2015. Effects of different anionic surfactants on methane hydrate formation. Chem. Eng. Sci. 13, 896–903.

Watanabe, K., Imai, S., Mori, Y.H., 2005a. Surfactant effects on hydrate formation in an unstirred gas/liquid system: an experimental study using HFC-32 and sodium dodecyl sulfate. Chem. Eng. Sci. 60, 4846–4857.

Watanabe, K., Niwa, S., Mori, Y.H., 2005b. Surface tensions of aqueous solutions of sodium alkyl sulfates in contact with methane under hydrate-forming conditions. J. Chem. Eng. Data 50, 1672–1676.

Yoslim, J., Linga, P., Englezos, P., 2010. Enhanced growth of methane-propane clathrate hydrate crystals with sodium dodecyl sulfate, sodium tetradecyl sulfate, and sodium hexadecyl sulfate surfactants. J. Cryst. Growth 313, 68–80.

Zhang, J.S., Lee, S., Lee, J.W., 2007a. Does SDS micellize under methane hydrate-forming conditions below the normal Krafft point? J. Colloid Interface Sci. 315, 313–318.

Zhang, J.S., Lee, S., Lee, J.W., 2007b. Solubility of sodium dodecyl sulfate near propane and carbon dioxide hydrate-forming conditions. J. Chem. Eng. Data 52 (6), 2480–2483.

Zhang, J.S., Lo, C., Somasundaran, P., Lee, J.W., 2010. Competitive adsorption between SDS and carbonate on tetrahydrofuran hydrates. J. Colloid Interface Sci. 341, 286–288.

Foaming property of the surfactants

Surfactants may cause foaming during the hydrate dissociation/gas recovery process, which could be a detrimental problem in practical applications. To evaluate the foaming capacity of the surfactants used, we performed the following experiments: 4 mL of solutions containing 10.4 $mol.m^{-3}$ of the surfactants SC_8S, $SC_{10}S$, $SC_{12}S$, $SC_{14}S$, and $SC_{16}S$ were prepared and introduced in test tubes. The test tubes were placed in a temperature-controlled bath at 275 K, and held at this temperature overnight. Then, the test tubes were vigorously mixed by hand shaking for 10 s. The figure below shows the amount of foam produced with the different surfactants. The snapshot was taken a few seconds after shaking the test tubes.

T = 275 K, and [C] = 10.4 $mol.m^{-3}$
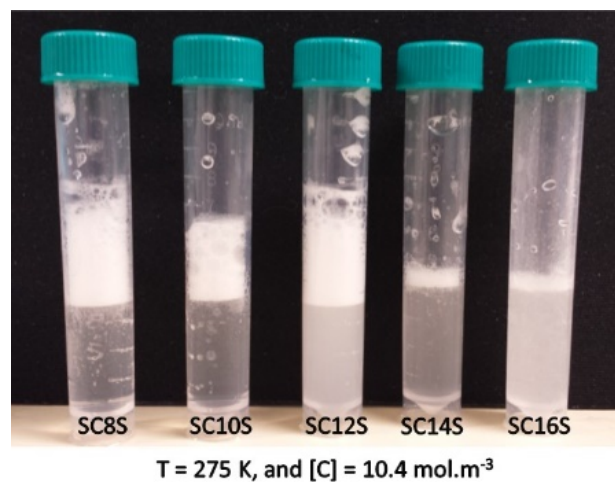
One can clearly observe that the height of foam is much lower for the surfactants $SC_{14}S$ and $SC_{16}S$. Therefore, using surfactants with more than 12 carbon atoms in their alkyl chain may avoid or limit foaming problem during hydrate decomposition in practical applications.

Effect of the starting pressure on hydrate growth rate

In the presented experiments, the degree of subcooling at the hydrate formation onset was the same (~ 5 K) for all systems, but the *pressure driving force* (difference between the starting pressure and the equilibrium pressure, at the experiment temperature (in our case 275 K)) was different. It was about 1.2 MPa for CO_2 and 1.9 MPa for CH_4. Such a difference in the pressure driving force might be responsible for the lower rate of hydrate formation observed for pure CO_2 hydrate.

To clarify this point, we conducted two additional experiments in which we evaluated the respective influence of the pressure driving force and the degree of subcooling on hydrate formation rate. In the first experiment, we used CH_4 at the starting pressure of 4.3 MPa (instead of 5.1 MPa) and T_{targ} = 273.25 K (instead of 275 K). The pressure driving force, and the degree of subcooling at T_{targ} were 1.58 MPa (instead of 1.94 MPa) and 4.7 K, respectively. In the second experiment, CH_4 was used at the starting pressure of 5.9 MPa and T_{targ} = 277 K. In this case, the pressure driving force, and the degree of subcooling at T_{targ} were 1.99 MPa and 4.3 K, respectively. In both experiments, the surfactant used was $SC_{12}S$ at the concentration of 10.4 mol.m^{-3}. The gas uptakes, $(n_{g,h})_{Tot}$ and rates of hydrate formation, $(\Delta n_{g,h}/\Delta t)_{Max}$ obtained are given in the table below along with the relative variation of the different parameters (given between brackets) calculated from the values for pure CH_4 presented in the manuscript.

The first additional experiment with CH_4 shows that a decrease of about 19% of the pressure driving force induced a decrease of about 14% of the gas uptake and the hydrate formation rate, at constant degree of subcooling. In the second experiment, the decrease of 8.5% of the degree of subcooling and the increase of about 3% of the pressure driving force led to an increase of about 6% of the gas uptake and a decrease of 16% of the hydrate formation rate.

These results confirm that the degree of subcooling affects more significantly the hydrate formation rate.

One can also remark that the hydrate formation rate obtained for pure CH_4 hydrate in the first new experiment remains much higher than that obtained for pure CO_2 hydrate.

Therefore, we do believe that the values of $(\Delta n_{g,h}/\Delta t)_{Max}$ obtained in this work are fairly representative of the intrinsic effect of the surfactant on the hydrate formation rate.

	Subcooling	"Pressure driving force"	$(n_{g,h})_{Tot}$	$(\Delta n_{g,h}/\Delta t)_{Max}$
	(K)	(MPa)	(mmol)	(mmol/min)
Pure CH_4 (manuscript)	4.7	1.94	318.1	8.62
Pure CH_4 (new experiment#1)	4.7	1.58	273.9	7.39
	(0)	(-18.6%)	(-13.9%)	(-14.3%)
Pure CH_4 (new experiment#2)	4.3	1.99	336.2	7.22
	(-8.5%)	(+2.6%)	(+5.7%)	(-16.2%)
Pure CO_2 (manuscript)	4.6	1.24	245.4	3.93